

PETROV-GALERKIN METHOD WITH LOCAL GREEN'S FUNCTIONS IN SINGULARLY PERTURBED CONVECTION-DIFFUSION PROBLEMS

OWE AXELSSON, EVGENY GLUSHKOV, AND NATALIA GLUSHKOVA

(Communicated by Peter Minev)

Abstract. Previous theoretical and computational investigations have shown high efficiency of the local Green's function method for the numerical solution of singularly perturbed problems with sharp boundary layers. However, in several space variables those functions, used as projectors in the Petrov-Galerkin scheme, cannot be derived in a closed analytical form. This is an obstacle for the application of the method when applied to multi-dimensional problems. The present work proposes a semi-analytical approach to calculate the local Green's function, which opens a way to effective practical application of the method. Besides very accurate approximation, the matrix stencils obtained with these functions allow the use of fast and stable iterative solution of the large sparse algebraic systems that arise from the grid-discretization. The advantages of the method are illustrated by numerical examples.

Key Words. Convection-diffusion equation, Petrov-Galerkin discretization, Fourier transform, integral equations, iterative solution.

1. Introduction

Singularly perturbed problems are generally acknowledged to be a hard task for numerical evaluation. Due to their solutions having sharp boundary and interior layers severe numerical instability can occur and a large error pollution spreads out over the whole domain as the perturbation parameter tends to its limit value.

A classical example of a singularly perturbed equation is the equation of the convection-diffusion problem:

$$(1.1) \quad \mathcal{L}u \equiv -\varepsilon\Delta u + \mathbf{b} \cdot \nabla u + cu = f, \quad (x, y) \in \Omega \subset \mathbb{R}^2$$

where ε is a small parameter and $c \geq 0$. Here we denote scalar products of algebraic vectors by dots, as in the convection term $\mathbf{b} \cdot \nabla u$, while the brackets notation is reserved for the scalar products in the functional Hilbert spaces occurring below.

Received by the editors February 4, 2004 and, in revised form, May 12, 2004.

2000 *Mathematics Subject Classification.* 65F10, 65N22, 65R10, 65R20.

We are thankful to Dr. B. Polman and Dr. S. Gololobov for the fruitful comments and useful remarks. The work was supported by the NWO-RFBR No. 047-008-007 and RFBR No. 03-01-96626 grants.

For the sake of definiteness let us consider a rectangular domain $\Omega : 0 \leq x \leq a_1, 0 \leq y \leq a_2$ with homogeneous Dirichlet boundary condition

$$(1.2) \quad u|_{\Gamma} = 0, \quad \Gamma = \partial\Omega.$$

Only the presence of the diffusion term $-\varepsilon\Delta u$ enables fulfillment of this condition at the outflow part Γ_- of the boundary Γ entailing a boundary layer of width $O(\varepsilon)$ near Γ_- (here $\Gamma_- = \{(x, y) \in \Gamma : \mathbf{b} \cdot \mathbf{n} > 0\}$, \mathbf{n} is an outward normal to $\partial\Omega$).

It is well known that if the standard Galerkin method, or the similar central difference method, is used in regions where layers occur, then unphysical oscillations arise. They can be suppressed by the use of a locally and significantly refined grid where a certain local Peclet number condition is satisfied [3]. Instead of the standard Galerkin method, the streamline upwind method (see [15]) is a popular method to stabilize the scheme. One more alternative to the Galerkin scheme, applicable to singularly perturbed problems, is the meshless local Petrov-Galerkin method [2].

Other methods used are related to the local characteristic line method, which is based on the property that away from the layers the solution follows narrowly the characteristic lines for the reduced equation ($\varepsilon = 0$), when ε is small. Using such methods with a proper locally refined grid, under certain assumptions regarding the influence of corner singularities, one can prove optimal order discretization error estimates, typically of $O(h^2)$, which hold uniformly in the singular perturbation parameter, see [4, 8, 18]. Other and related papers can be found in [16].

Among the variety of approaches to regularization of singularly perturbed problems there is a group of methods based on the use of Green's functions associated with the equations considered. Different kinds of Green's functions are used for preconditioning [12] or for construction the fine-scale spaces in the multiscale stabilized methods [9]. The present paper deals with the method [5], which may be considered as a special case of the approach [2] with the local Green's functions used as projectors (test space). In distinction to the global Green's functions used in [12], the local ones are set on elementary supports defined by discretization. On the other hand, unlike to the fine-scale Green's functions of the multiscale decomposition methods, they are connected with a coarse mesh and do not possess, therefore, the property to provide an hierarchical exact basis of the infinitely dimension fine-scale spaces. Nevertheless, the local Green's functions also provide the stabilization effect by accounting *indirectly* for the fine-scale behavior. In this regard the method proposed may be treated as a specific implementation of the multiscale decomposition theory [10].

Let us give the main idea of the presented approach with a simple example of a uniform grid approximation. Let

$$(1.3) \quad u_h(x, y) = \sum_{k=1}^N u_k \varphi_k(x, y)$$

be an expansion of the exact solution of the problem (1.1) and (1.2) in terms of basis functions $\varphi_k = \varphi((x - x_k)/h, (y - y_k)/h)$ defined at the interior nodes (x_k, y_k) of a grid covering Ω with a step h (Fig. 1); $\varphi(x, y)$ is a shape-function. In line with the Petrov-Galerkin scheme, the unknown coefficients u_k are determined from the

variational condition

$$(1.4) \quad (\mathcal{L}u_h - f, \psi_l) = 0, \quad l = 1, 2, \dots, N,$$

where the set of projectors $\{\psi_l\}_{l=1}^N$ is dense as $N \rightarrow \infty$ in the Hilbert space with the scalar product of eq. (1.4). We take here the L_2 space with the product $(f, g) = \iint f g^* dx dy$ (an asterisk, hereinafter, will indicate complex conjugate values and adjoint operators).

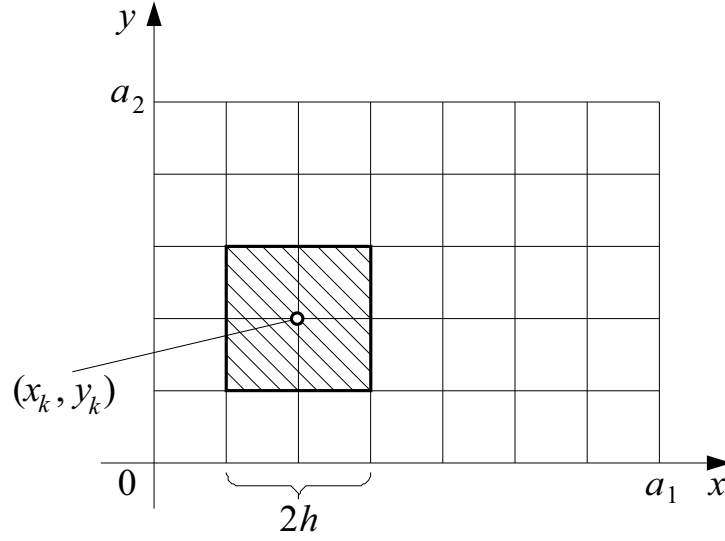


FIGURE 1

Using the adjoint operator $\mathcal{L}^* : (\mathcal{L}u, v) = (u, \mathcal{L}^*v)$ the variational equality (1.4) can be converted into the form

$$(1.5) \quad (u_h - u, \mathcal{L}^*\psi_l) = 0.$$

If the shape-function ψ of the projectors $\psi_l = \psi(x - x_l, y - y_l)$ complies with the equality

$$(1.6) \quad \mathcal{L}^*\psi = \delta, \quad (x, y) \in \omega$$

where $\delta(x, y)$ is Dirac's delta-function, then it follows from (1.5) that the approximate and the exact solutions coincide at the nodes:

$$(1.7) \quad u_h(x_l, y_l) = u(x_l, y_l).$$

In eq. (1.6) ω is a finite support of ψ . For a uniform grid projectors ψ_l are localized in $2h \times 2h$ squares centered at the nodes (Fig. 1), i.e. in such a case $\omega = \omega_h$ is a square $|x| \leq h, |y| \leq h$. In accordance with the general scheme ψ must satisfy the natural boundary condition

$$(1.8) \quad \psi|_{\Gamma_h} = 0,$$

where Γ_h is the boundary of ω_h .

With equation (1.1) integration by parts yields

$$(1.9) \quad (\mathcal{L}(u_h - u), \psi) = (u_h - u, \hat{\mathcal{L}}\psi) + \oint_{\partial\omega} \varepsilon \frac{\partial\psi}{\partial n} (u_h - u) d\Gamma_h$$

where $\hat{\mathcal{L}}: \hat{\mathcal{L}}u = -\varepsilon\Delta u - \nabla \cdot (\mathbf{b}u) + cu$ is the main differential part of \mathcal{L}^* . The operator \mathcal{L}^* cannot be written here explicitly, so *the local Green's function* ψ is defined as a solution of the equation

$$(1.10) \quad \hat{\mathcal{L}}\psi = \delta, \quad (x, y) \in \omega_h$$

with the boundary condition (1.8) [3].

In practice the local Green's function method exhibits high accuracy at the nodes even with a coarse grid. It is further of significant importance that appearance of the layers as $\varepsilon \rightarrow 0$ does not degrade its numerical stability. Besides the theoretical heuristic calculations above, this fact was shown numerically as well, however, only with 1D examples [7, 3]. Extension of the method to several variables has been restrained by the absence of an analytical solution of the problem (1.10), (1.8) for such a case. The present work gives an example of an effective computer implementation of the method in 2D by using a semi-analytical Fourier-transform technique.

It is pertinent to note that the local Green's function can be given not only in a square. Since its main property is to give a delta-function in eq. (1.5), we can vary the shape of ω_h regardless of supports of trial functions. It is only important to set the test local Green's functions at points, where coincidence (1.7) should be achieved.

We start from the square support ω_h , which goes together with a uniform grid discretization, just to demonstrate that the method works and works well without any mesh refinement in the layer parts of the domain. If more points within a layer are desirable, one can take, for example, rectangular supports with arbitrary large aspect ratio. This allows one to adjust the mesh in the layers along straight lines to become arbitrarily thin along the layer. The generalization of the technique given below on such a case is obvious. It would only require to use two mesh values h_1, h_2 instead of h in eqs. (2.8) – (2.15) and further on.

As the most promising with a non-uniform (non-polygonal) mesh we mention the use of circle and elliptic supports. Solution of integral equations at $\partial\omega$ and derivation of integral's asymptotics as $\varepsilon \rightarrow 0$ (see Section 2) can be much easier for such subdomains with smooth boundaries than for polygonal elements with corner points.

In this paper we give, first, an idea of the technique proposed with an 1D example (subsection 2.1), extending then its application to the 2D case (subsection 2.2). The local Green's function $\psi(x, y)$ is derived in terms of integrals with respect to the unknown normal derivative $\partial\psi/\partial n$ at Γ_h . The latter, in turn, is approximated by orthogonal polynomials. Then, in Section 3, we derive the computational formulae for the Petrov-Galerkin method arriving at a matrix stencil also expressed in terms of $\partial\psi/\partial n$. Some numerical test examples are given in Section 4. Finally, stability bounds and a hybrid method are discussed in Section 5.

2. Integral representation of the local Green's functions

For an efficient derivation of the local Green's functions we use the Fourier transform technique. The Fourier transform pair

$$(2.1) \quad \begin{cases} \mathcal{F}[u] \equiv \int_{R^n} u(\mathbf{x}) e^{i\boldsymbol{\alpha} \cdot \mathbf{x}} d\mathbf{x} = U(\boldsymbol{\alpha}) \\ \mathcal{F}^{-1}[U] \equiv \frac{1}{(2\pi)^n} \int_{R^n} U(\boldsymbol{\alpha}) e^{-i\boldsymbol{\alpha} \cdot \mathbf{x}} d\boldsymbol{\alpha} = u(\mathbf{x}) \end{cases}$$

$$\mathbf{x} = (x_1, x_2, \dots, x_n), \quad \boldsymbol{\alpha} = (\alpha_1, \alpha_2, \dots, \alpha_n), \quad \boldsymbol{\alpha} \cdot \mathbf{x} = \sum_i^n \alpha_i x_i$$

can only be applied to differential equations with constant coefficients. However, since the discretization step h is assumed to be much smaller than the characteristic scales of the variation of the coefficients, we can approximate $\mathbf{b}(\mathbf{x})$ and $c(\mathbf{x})$ in eq. (1.1) by piece-wise functions, which are constant within element subdomains (the so called freezing coefficients concept). In this case we take $\nabla \cdot (\mathbf{b}\psi) = \mathbf{b} \cdot \nabla \psi$ with $\mathbf{b} = \text{const}$ in eq. (1.6). By virtue of the variational statement of the problem, below we treat operator \mathcal{F} as a generalized Fourier transform applicable to distributions (Dirac's δ -functions) as well.

2.1. 1D case. To get an idea of the method proposed, let us first apply the transform to the 1D two-point problem (1.6), (1.8), whose solution is actually easily derived by other means, as well. Application of the transform presumes that a function is defined in the whole space R^n , so we extend $\psi(x)$ to the exterior of the interval $|x| \leq h$ by zero. In this case the points $x = \pm h$ are the points of discontinuity for derivatives $\psi^{(m)}(x)$, $m \geq 1$ ($\psi(x)$ is continuous due to the boundary condition (1.8): $\psi(\pm h) = 0$). Fourier transform of derivatives of non-smooth functions obeys the following rule:

$$\mathcal{F}[u^{(m)}] = (-i\alpha)^m U(\alpha) + (u_{m-1} - i\alpha u_{m-2} + \dots + (-i\alpha)^{m-1} u_0) e^{i\alpha x_0},$$

where $U(\alpha) = \mathcal{F}[u]$, x_0 is a point of discontinuity and $u_k = \lim_{\delta \rightarrow 0} [u^{(k)}(x_0 - \delta) - u^{(k)}(x_0 + \delta)]$, $0 \leq k \leq m-1$ are values of the jumps of the derivatives at x_0 . Therefore, the Fourier transform brings (1.6), extended by zero onto the whole axis, to the functional equation

$$(2.2) \quad \mathcal{F}[\hat{\mathcal{L}}\psi] = L(\alpha)\Psi(\alpha) - v^+ e^{i\alpha h} + v^- e^{-i\alpha h} = 1.$$

Here, $L(\alpha) = \varepsilon\alpha^2 + i\alpha b + c$; $v^\pm = \varepsilon\psi'(\pm h \mp 0)$ are unknown constants, which have to be taken to meet the boundary conditions $\psi(\pm h) = 0$.

From (2.2) we get immediately

$$\Psi(\alpha) = G(\alpha)(1 + v^+ e^{i\alpha h} - v^- e^{-i\alpha h}), \quad G(\alpha) = 1/L(\alpha),$$

and then

$$(2.3) \quad \psi(x) = \mathcal{F}^{-1}[\Psi(\alpha)] = g(x) + v^+ g(x-h) - v^- g(x+h),$$

where

$$(2.4) \quad g(x) = \mathcal{F}^{-1}[G] = \frac{1}{2\pi} \int_{-\infty}^{\infty} G(\alpha) e^{-i\alpha x} d\alpha$$

is the *global* Green's function of (1.6) in 1D.

An explicit representation of $g(x)$ is easily derived from the integral (2.4) by means of the residual technique for path integrals. There are two pure imaginary poles of $G(\alpha)$ (roots of the denominator $L(\alpha) = \varepsilon(\alpha - \zeta_1)(\alpha - \zeta_2)$) located in the upper and lower half-planes of the complex plane α :

$$\zeta_{1,2} = i(-b \pm \sqrt{b^2 + 4\varepsilon c})/2\varepsilon$$

In accordance with Jordan's lemma and Cauchy's theorem [13], the contribution of the residuals at poles ζ_1 for $x \leq 0$ and ζ_2 for $x \geq 0$ yields

$$(2.5) \quad g(x) = \frac{i}{\varepsilon(\zeta_1 - \zeta_2)} \left\{ \begin{array}{ll} e^{-i\zeta_1 x}, & x \leq 0 \\ e^{-i\zeta_2 x}, & x \geq 0 \end{array} \right\} \sim \frac{1}{b} \left\{ \begin{array}{ll} e^{cx/b}, & x \leq 0 \\ e^{-(b^2+ce)x/\varepsilon b}, & x \geq 0 \end{array} \right\}$$

as $\varepsilon \rightarrow 0$. For small ε , the function $g(x)$ demonstrates a typical layer behaviour at the right (upwind) side of the source-point $x = 0$ and an independent of ε decrease for $x < 0$ (the dash-point line in the example shown in Fig. 2). Consequently, in (2.3) the term $g(x+h)$ has a layer at $x = -h$ while $g(x-h)$ does not contribute to any sharp layer of $\psi(x)$ (dashed lines). After fixing the values v^\pm from the condition $\psi(\pm h) = 0$, the total plot of $\psi(x)$ takes the form shown by the solid line in Fig. 2.

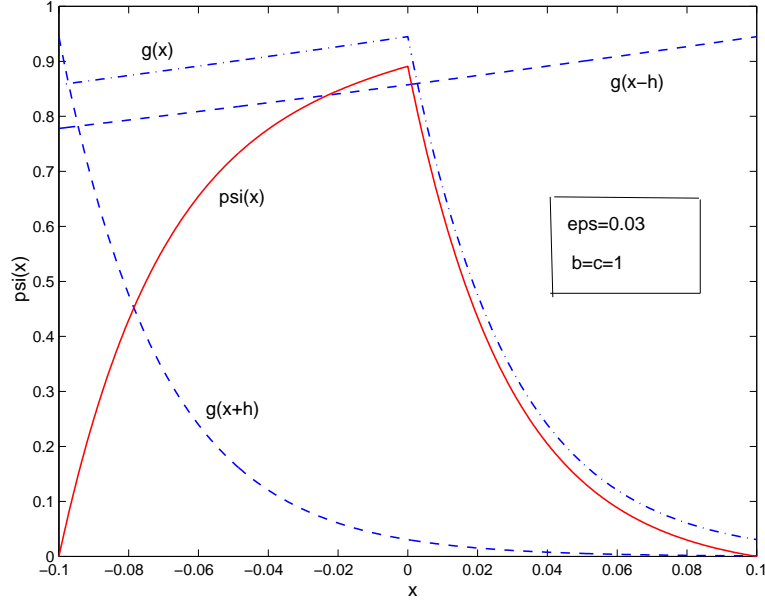


FIGURE 2. 1D local Green's function

It may seem attractive to design $\psi(\mathbf{x})$ in 2D using 1D functions of the form (2.3) taken, for example, along the characteristics of $\hat{\mathcal{L}}$. However, it cannot be performed analytically. Moreover, since in several variables $\mathbf{x} = 0$ is a singular point (with a logarithmic singularity in 2D: $g(\mathbf{x}) \sim g_0 \ln |\mathbf{x}|$, as $|\mathbf{x}| \rightarrow 0$), any approximation by such functions would be qualitatively mismatched. Special methods for $\psi(\mathbf{x})$ designed in R^n , $n \geq 2$ must therefore be developed.

2.2. 2D case. Similarly to the above, application of the Fourier transform to (1.6) in the entire space R^2 yields the explicit integral representation for the global Green's function $g(x, y)$:

$$(2.6) \quad g(\mathbf{x}) = \frac{1}{(2\pi)^2} \int_{-\infty}^{\infty} \int_{-\infty}^{\infty} G(\boldsymbol{\alpha}) e^{-i\boldsymbol{\alpha} \cdot \mathbf{x}} d\boldsymbol{\alpha}, \quad G(\boldsymbol{\alpha}) = 1/L(\boldsymbol{\alpha}),$$

$$L(\boldsymbol{\alpha}) = \varepsilon|\boldsymbol{\alpha}|^2 + i\boldsymbol{\alpha} \cdot \mathbf{b} + c.$$

It, however, can be simplified to one-fold integrals only:

$$(2.7) \quad g(x, y) = \frac{1}{2\pi} \int_{-\infty}^{\infty} \begin{cases} G_1(\alpha_2, x) e^{-i\alpha_2 y} d\alpha_2, & |x| \geq |y| \\ G_2(\alpha_1, y) e^{-i\alpha_1 x} d\alpha_1, & |y| \geq |x| \end{cases}$$

$$G_n(\alpha, x_n) = \exp[-(b_n x_n + d_n |x_n|)/2\varepsilon]/d_n, \quad n = 1, 2$$

$$d_n(\alpha) = \sqrt{b_n^2 + 4\varepsilon(\varepsilon\alpha^2 + i\hat{b}_n\alpha + c)}, \quad \hat{b}_n = \begin{cases} b_2, & n = 1 \\ b_1, & n = 2 \end{cases}$$

(whenever no confusion can arise, we write α instead of α_1 or α_2 for the components of $\boldsymbol{\alpha}$ and x, y instead of x_1, x_2 for the \mathbf{x} ones). Further simplification of these integrals in line with the residual technique is impossible due to the branch points of $d_n(\alpha)$ and the branch cuts implied in the complex plane α , although a close analytical form of $g(x, y)$ has been derived by other way as well [14].

When $r = \sqrt{x^2 + y^2} \rightarrow 0$, as expected, these integrals become divergent in accordance with the logarithmic singularity of $g(x, y)$.

We remark that selection of the integrals in (2.7) depending on the $|x|, |y|$ ratio is not mandatory. It only provides its faster convergence at infinity (as $\alpha \rightarrow \infty$).

If ψ is considered to be extended by zero from ω_h onto the whole plane R^2 , eq. (1.10) takes in the Fourier transform domain the following form:

$$(2.8) \quad \Psi(\boldsymbol{\alpha}) = G(\boldsymbol{\alpha}) \{1 + V_x^+(\alpha_2) e^{i\alpha_1 h} - V_x^-(\alpha_2) e^{-i\alpha_1 h} + V_y^+(\alpha_1) e^{i\alpha_2 h} - V_y^-(\alpha_1) e^{-i\alpha_2 h}\}.$$

Here $V_x^\pm = \mathcal{F}[v_x^\pm]$ and $V_y^\pm = \mathcal{F}[v_y^\pm]$, where $v_x^\pm(y)$ and $v_y^\pm(x)$ are unknown normal derivatives $\varepsilon\partial\psi/\partial x$ and $\varepsilon\partial\psi/\partial y$ at the square sides $x = \pm h$ and $y = \pm h$, respectively. Fourier inversion of (2.8) implies

$$(2.9) \quad \psi = g + u_x^+ - u_x^- + u_y^+ - u_y^-$$

with functions

$$(2.10) \quad \begin{cases} u_x^\pm(x, y) = \frac{1}{2\pi} \int_{-\infty}^{\infty} G_1(\alpha, x \mp h) V_x^\pm(\alpha) e^{-i\alpha y} d\alpha = \int_{-h}^h g(x \mp h, y - t) v_x^\pm(t) dt \\ u_y^\pm(x, y) = \frac{1}{2\pi} \int_{-\infty}^{\infty} G_2(\alpha, y \mp h) V_y^\pm(\alpha) e^{-i\alpha x} d\alpha = \int_{-h}^h g(x - t, y \mp h) v_y^\pm(t) dt \end{cases}$$

expressed in terms of the unknown v_x^\pm and v_y^\pm .

In view of boundary condition (1.8), these unknowns have to comply with the integral equations

$$(2.11) \quad \begin{cases} (u_x^+ - u_x^- + u_y^+ - u_y^-)|_{x=\pm h} = -g(\pm h, y), & |y| \leq h \\ (u_x^+ - u_x^- + u_y^+ - u_y^-)|_{y=\pm h} = -g(x, \pm h), & |x| \leq h \end{cases}$$

A semi-analytical solution of these equations can be obtained in terms of certain basis functions $p_k(t)$, $|t| \leq h$:

$$(2.12) \quad \begin{cases} v_x^\pm(y) = \sum_{k=0}^{\infty} c_k^\pm p_k(y), & |y| \leq h \\ v_y^\pm(x) = \sum_{k=0}^{\infty} t_k^\pm p_k(x), & |x| \leq h \end{cases}$$

if Galerkin's scheme of discretization is applied to (2.11).

Since the unknowns are expected to be continuous functions, the usual Fourier exponents $e^{\pm i\pi kt/h}$ or splines are quite acceptable as a basis. However, orthogonal polynomials with a weight accounting for the behaviour at the ends of the approximation interval provide generally a better convergence. For the numerical examples below we have selected $p_k(t) = (h^2 - t^2)P_k^{(1,1)}(t/h)$ as the basis and $q_l(t) = P_l(t/h)$ as test functions ($P_k^{(\alpha,\beta)}(x)$, $P_l(x)$ are Jacobi's and Legendre polynomials [1]).

Galerkin's variational procedure reduces eqs. (2.11) to the linear algebraic system

$$(2.13) \quad \sum_{k=0}^M A_{lk} \mathbf{t}_k = \mathbf{f}_l, \quad l = 0, 1, 2, \dots, M$$

for the unknown expansion coefficients $\mathbf{t}_k = \{c_k^+, c_k^-, t_k^+, t_k^-\}$; M fixes the number of terms kept in expansion (2.12). With the basis and projectors selected the 4×4 matrix-blocks A_{lk} and the right-hand side vectors \mathbf{f}_l take the following form

$$(2.14) \quad A_{lk} = \begin{bmatrix} a_{1,lk}(0) & -a_{1,lk}(2h) & b_{2,lk}^+(h) & -b_{2,lk}^-(h) \\ a_{1,lk}(-2h) & -a_{1,lk}(0) & b_{2,lk}^+(-h) & -b_{2,lk}^-(-h) \\ b_{1,lk}^+(h) & -b_{1,lk}^-(h) & a_{2,lk}(0) & -a_{2,lk}(2h) \\ b_{1,lk}^+(-h) & -b_{1,lk}^-(-h) & a_{2,lk}(-2h) & -a_{2,lk}(0) \end{bmatrix}$$

$$\mathbf{f}_l = [f_{1,l}^+ \ f_{1,l}^- \ f_{2,l}^+ \ f_{2,l}^-]^T$$

where

$$(2.15) \quad \begin{cases} a_{n,lk}(2p) = \frac{1}{2\pi} \int_{-\infty}^{\infty} G_n(\alpha, 2p) P_k(\alpha) Q_l(\alpha) d\alpha \\ b_{n,lk}^\pm(p) = \frac{1}{2\pi} \int_{-\infty}^{\infty} e_n^\pm(\alpha) P_k(\alpha) Q_l(z_n^\pm) e^{-i\alpha p} d\alpha \\ f_{n,l}^\pm = -\frac{1}{2\pi} \int_{-\infty}^{\infty} G_n(\alpha, \pm h) Q_l(\alpha) d\alpha \end{cases}$$

$$p = 0, \pm h; \quad n = 1, 2; \quad z_n^\pm = i(\pm d_n - b_n)/2\varepsilon$$

$$e_n^\pm(\alpha) = \exp((-d_n \pm b_n)\lambda/2)/d_n, \quad \lambda = h/\varepsilon$$

$$G_n(\alpha, x_n), \quad d_n(\alpha) \text{ as in eq. (2.7);}$$

$$P_k(\alpha) = \mathcal{F}[p_k] = i^k 4(k+1)h^2 j_{k+1}(\alpha h)/\alpha$$

$$Q_l(\alpha) = \mathcal{F}[q_l(\alpha)]^* = i^{-l} 2h j_l(\alpha h);$$

$j_m(z) = \sqrt{2\pi/z} J_{m+1/2}(z)$ are spherical Bessel functions [1].

Despite the fact that integrals (2.15) are improper ones given over an infinite interval, due to factors like $e^{-d_n \lambda}$ their convergence is very fast, although certain a priori analytical calculation aiming to adjust them to the numerical integration has to be carried out. Moreover, if $\varepsilon \ll 1$ and, consequently, $\lambda = h/\varepsilon$ is very large, the exponential behavior of the integrands permits very good approximation of the integrals by saddle point asymptotics, derived using the steepest descent method [6].

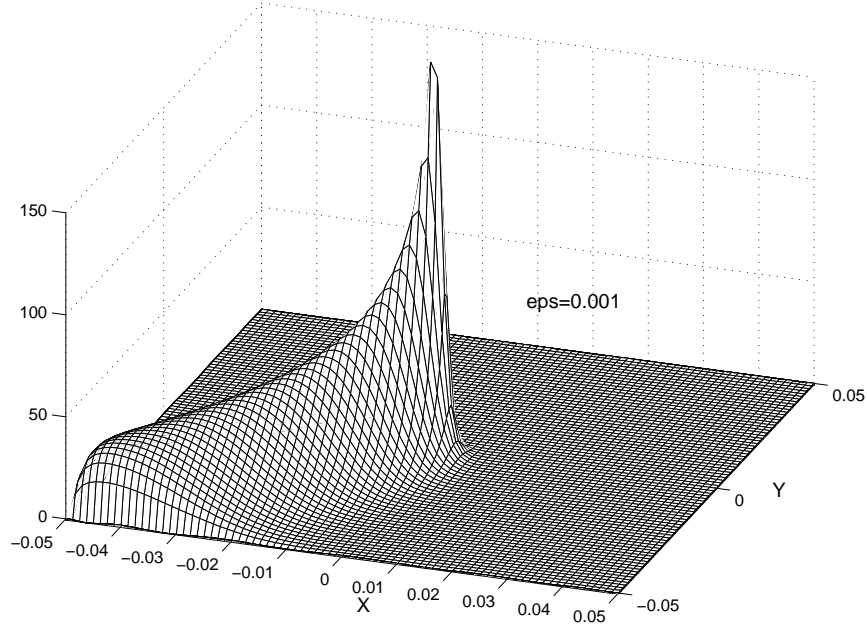


FIGURE 3. 2D local Green's function

An example of the shape function $\psi(x, y)$ computed in line with the scheme above for $\varepsilon = 0.001, h = 0.05, c = 1$ and a diagonal velocity field $\mathbf{b} = \{\sqrt{2}, \sqrt{2}\}/2$ is given in Fig. 3. Similar to the 1D example above one can see a sharp decrease at the upwind side of the source-point $\mathbf{x} = 0$ and boundary layers at the outflow part of the edges $x = -0.05$ and $y = -0.05$ (for the backward flux $-\mathbf{b}$ associated with the adjoint operator $\hat{\mathcal{L}}$). The growth in accordance with the logarithmic singularity at $\mathbf{x} = 0$, which does not appear in the 1D case, is also clearly seen here.

However, it is important to note the fact that we do not need $\psi(x, y)$ itself, but due to the integral technique used, the matrix stencil we seek can be obtained merely in terms of the auxiliary functions v_x^\pm and v_y^\pm .

3. The matrix-stencil

The variational equality (1.4) results in an algebraic system

$$(3.1) \quad \sum_{k=1}^N a_{lk} u_k = f_l, \quad l = 1, 2, \dots, N,$$

where $a_{lk} = (\mathcal{L}\varphi_k, \psi_l)$, $f_l = (f, \psi_l)$, and u_k are unknown coefficients in expansion (1.3). The generalized Parseval's identity $(f, g) = \frac{1}{(2\pi)^2} (F, G)$ makes it possible to evaluate the components a_{lk} in the Fourier transform domain:

$$(3.2) \quad a_{lk} = \frac{1}{(2\pi)^2} (\mathcal{F}[\mathcal{L}\varphi_k], \Psi_l).$$

Here $\mathcal{F}[\mathcal{L}\varphi_k] = L(\boldsymbol{\alpha})\Phi_k(\boldsymbol{\alpha})$ and $\Psi_l(\boldsymbol{\alpha}) = \mathcal{F}[\psi_l] = \Psi(\boldsymbol{\alpha})e^{i(\alpha_1 x_l + \alpha_2 y_l)}$, all the functions are assumed to be extended by zero beyond their supports.

Let the basis shape-function φ be designed from the traditional hat functions:

$$(3.3) \quad \varphi(x, y) = \varphi(x)\varphi(y), \quad \varphi(t) = \begin{cases} 1 - |t|, & |t| \leq 1 \\ 0, & |t| > 1 \end{cases},$$

so that $\Phi_k(\boldsymbol{\alpha}) = \mathcal{F}[\varphi_k] = h^2 \Phi(\alpha_1 h) \Phi(\alpha_2 h) e^{i(\alpha_1 x_k + \alpha_2 y_k)}$ with $\Phi(\alpha) = \mathcal{F}[\varphi]$. Since the function $G(\boldsymbol{\alpha})$, involved in the representation (3.2) through $\Psi(\boldsymbol{\alpha})$ of form (2.8), is the inverse to $L(\boldsymbol{\alpha})$: $L(\boldsymbol{\alpha})G(\boldsymbol{\alpha}) = 1$, this representation can be simplified to the following form:

$$(3.4) \quad a_{lk} = \delta(l - k) + a_{lk,x}^+ - a_{lk,x}^- + a_{lk,y}^+ - a_{lk,y}^-,$$

where $\delta(p) = \begin{cases} 1, & p = 0 \\ 0, & p \neq 0 \end{cases}$ is the Kronecker delta,

$$(3.5) \quad \begin{cases} a_{lk,x}^\pm = \delta(p_1 \pm 1) I_{p_2}^\pm \\ a_{lk,y}^\pm = \delta(p_2 \pm 1) J_{p_1}^\pm \end{cases}$$

$$(3.6) \quad \begin{cases} I_{p_2}^\pm = \int_{-h}^h v_x^\pm(y) \varphi(y/h + p_2) dy \\ J_{p_1}^\pm = \int_{-h}^h v_y^\pm(x) \varphi(x/h + p_1) dx \end{cases}$$

$$I_{p_2}^\pm, J_{p_1}^\pm \equiv 0 \text{ for } |p_n| \geq 2, \quad n = 1, 2$$

$$p_1 = (x_l - x_k)/h, \quad p_2 = (y_l - y_k)/h, \quad p_n = 0, \pm 1;$$

The restriction $|p_n| \leq 1$ means that only nodes (x_k, y_k) adjacent to (x_l, y_l) contribute to a_{lk} . The structure of the three by three matrix-stencil $B = [b(p_1, p_2)]$,

fixing components a_{lk} in line with the rule $a_{lk} = b(p_1, p_2)$, $p_n = -1, 0, 1$, is therefore easily seen:

$$(3.7) \quad B = \begin{bmatrix} I_{-1}^+ + J_{-1}^+ & I_0^+ & I_1^+ - J_{-1}^- \\ J_0^+ & 1 & -J_0^- \\ -I_{-1}^- + J_1^+ & -I_0^- & -I_1^- - J_1^- \end{bmatrix}$$

This stencil structure follows also directly from the representation obtained by the integration by parts (see (1.9)):

$$a_{lk} = (\varphi_k, \hat{\mathcal{L}}\psi_l) + \oint_{\partial\omega_l} \varepsilon \frac{\partial\psi_l}{\partial n} \varphi_k d\Gamma_l.$$

As soon as the expansion coefficients \mathbf{t}_k have been determined from the system (2.13), calculation of the entries of the B -matrix through integrals (3.6) does not take any major part in the total computing time.

Besides that, representation (3.7) is helpful for analyzing general properties of the sparse-matrix $A = [a_{lk}]$ with regards to iterative solution of system (3.1). Since $\partial\psi/\partial n < 0$ at Γ_h (due to decrease of ψ from positive values to zero when approaching to the edges) all entries of B , except $b(0,0) = 1$, are negative. It results in negative off-diagonal components of A , so that A is an M -matrix if it is diagonally dominant [17] (see also subsection 5.1).

4. Numerical examples

4.1. Boundary layers. As an example let us consider problem (1.1) - (1.2) in the unit square $0 \leq x, y \leq 1$ with the right-hand side function $f(x, y)$ generated by the exact solution

$$(4.1) \quad u(x, y) = x^2 y^2 (1 - e_1(x))(1 - e_2(y))$$

$$e_n(x_n) = \exp(-(1 - x_n)/\varepsilon), \quad n = 1, 2 \quad x_1 = x, \quad x_2 = y$$

with boundary layers at the sides $x = 1$ and $y = 1$.

In actual computation $f(x, y)$ was replaced by a piecewise function, so that the components f_l in system (3.1) were approximated as follows

$$f_l = (f, \psi_l) \approx f(x_l, y_l) \iint \psi_l d\Omega = f(x_l, y_l) [1 + 4(c_0^+ - c_0^- + t_0^+ - t_0^-)/3]/c$$

(if $c = 0$ the method is also applicable but with another form of the right hand side f_l).

The coefficients in (1.1) are assumed to be constant; $c = 1$ in all the cases. The velocity vector \mathbf{b} has unit length: $|\mathbf{b}| = 1$, its direction is defined by the angle $\theta : \mathbf{b} = (\cos \theta, \sin \theta)$. In this case the Peclet number is equal to $h/(2\varepsilon)$.

The examples given in the Tables 1 and 2 show how the matrix-stencil B and the solution get stabilized as $\varepsilon \rightarrow 0$, despite the sharp boundary layers occurring in the exact solution (4.1).

In these tables elements of the matrix-stencil B , the number of Seidel iterations for system (3.1), the average nodal error and the computing time are given depending on the singular parameter ε . We keep only four digits in the elements of B , so that zero ones are in reality small but non-zero. The number of iterations

was determined by the relative accuracy 10^{-11} . The error $r_h = \int |u - u_h| d\Omega$ is approximated by the nodal sum: $h^2 \sum_k |u(x_k, y_k) - u_h(x_k, y_k)|$, $h^2 = 1/N$. The number of grid cells in these examples was $N = 100 \times 100$, that is $h = 0.01$. The number of expansion terms M (see eqs. (2.12, 2.13) in all examples was taken to be equal to 10. Table 1 is for the velocity parallel to the x-axis: $\theta = 0$, while table 2 is for $\theta = \pi/8$.

The computations were carried out at a PC with the processor speed 733 MHz. The increase of the total computing time for very small values of ε is due to the costs of the numerical calculation of the integrals (2.15). As was mentioned above, these computing expenses are practically reduced to zero (no more then 1 sec. for $\varepsilon \leq 10^{-5}$ in the examples of Tables 1-3) when those integrals are replaced by their asymptotic expressions derived in [6].

Table 1, $\theta = 0$

ε	matrix-stencil B			number of iterations	error r_h	time
10^{-1}	-0.0843	-0.1543	-0.0843	990	0.0057	14 sec.
	-0.1622	1.0000	-0.1622			
	-0.0909	-0.1705	-0.0909			
10^{-2}	-0.0563	-0.0914	-0.0563	301	0.0046	5 sec.
	-0.1528	1.0000	-0.1528			
	-0.1196	-0.2485	-0.1196			
10^{-3}	-0.0002	-0.0000	-0.0002	40	0.0058	2 sec.
	-0.0128	1.0000	-0.0128			
	-0.1596	-0.2485	-0.1596			
10^{-5}	-0.0000	-0.0000	-0.0000	17	0.0030	6 sec.
	-0.0000	1.0000	-0.0000			
	-0.0292	-0.9315	-0.0292			
10^{-7}	-0.0000	-0.0000	-0.0000	16	0.0028	29 sec.
	-0.0000	1.0000	-0.0000			
	-0.0255	-0.9389	-0.0255			
10^{-9}	-0.0000	-0.0000	-0.0000	16	0.0028	113 sec.
	-0.0000	1.0000	-0.0000			
	-0.0255	-0.9390	-0.0255			

Table 2, $\theta = \pi/8$

ε	matrix-stencil B	number of iterations	error r_h	time
10^{-1}	-0.0834 -0.1549 -0.0858 -0.1591 1.0000 -0.1653 -0.0894 -0.1699 -0.0920	4950	0.0113	66 sec.
10^{-2}	-0.0498 -0.0952 -0.0673 -0.1259 1.0000 -0.1846 -0.1011 -0.2397 -0.1336	282	0.0039	5 sec.
10^{-3}	-0.0000 -0.0001 -0.0012 -0.0016 1.0000 -0.0743 -0.0454 -0.5184 -0.3490	21	0.0021	2 sec.
10^{-5}	-0.0000 -0.0000 -0.0000 -0.0000 1.0000 -0.0000 -0.0039 -0.5717 -0.4136	9	0.0030	7 sec.
10^{-7}	-0.0000 -0.0000 -0.0000 -0.0000 1.0000 -0.0000 -0.0050 -0.5695 -0.4147	9	0.0025	43 sec.
10^{-9}	-0.0000 -0.0000 -0.0000 -0.0000 1.0000 -0.0000 -0.0050 -0.5695 -0.4147	9	0.0025	116 sec.

The next table demonstrates how convergence, accuracy and computing time depend on the grid size h .

Table 3 for $\varepsilon = 0.0001$, $\theta = \pi/8$

grid $N_1 \times N_2 = N$	grid size h	number of iterations	error r_h	total time
$100 \times 100 = 10^4$	0.01	6	0.00353	3 sec.
$200 \times 200 = 4 \cdot 10^4$	0.005	9	0.00172	3 sec.
$300 \times 300 = 9 \cdot 10^4$	0.0033	11	0.00100	8 sec.
$400 \times 400 = 16 \cdot 10^4$	0.0025	20	0.00066	14 sec.
$500 \times 500 = 25 \cdot 10^4$	0.0020	27	0.00036	25 sec.

4.2. Interior layers. The examples above show that the method behaves stably despite the presence of boundary layers. However, since generally there were no mesh points in the layers, it can make a false impression that the algorithm is only applicable in regions where the reduced first order problem approximates the exact solution. To demonstrate that it has the same favorable accuracy properties in other regions we include the next test example with interior layers (Fig. 4). Here the equation (1.1) is homogeneous ($f \equiv 0$) but with an inhomogeneous boundary condition at the inflow part Γ_+ instead of (1.2): $u|_{\Gamma} = u_0$ where $u_0 = 1$ for $x = 0$, $0.25 \leq y \leq 0.5$ and $u_0 \equiv 0$ for the rest of Γ .

To take into account this inhomogeneous condition, we add a *known* function $u_{0,h}$: $u_{0,h}|_{\Gamma} = u_0$ to u_h of form (1.3). By doing so, the matrix $[a_{lk}]$ of the system

(3.1) remains the same, while $u_{0,h}$ only changes the right hand side into $f_l = -(\mathcal{L}u_{0,h}, \psi_l)$.

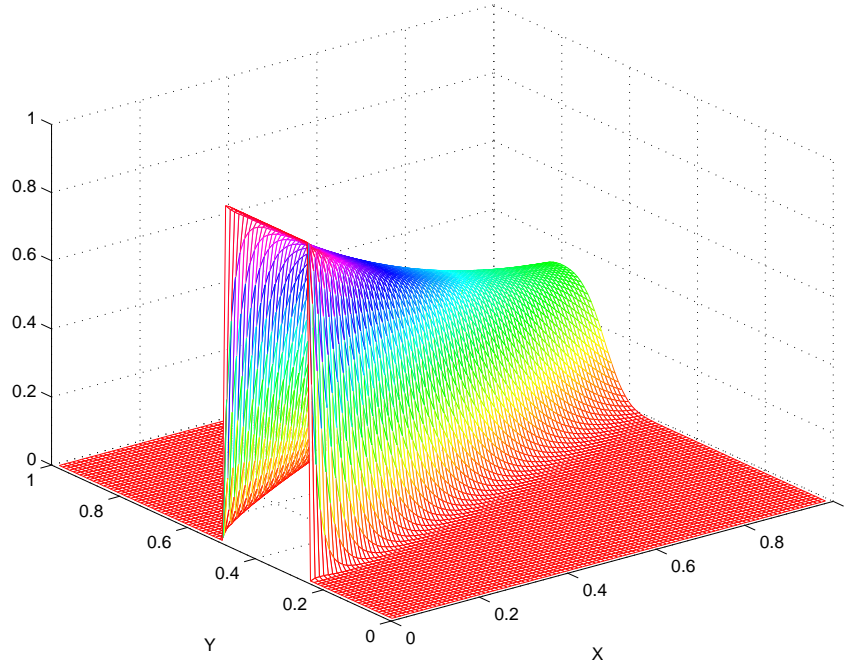


FIGURE 4. Test example with interior layers emanating from the points of discontinuity of the boundary condition at the inflow side; $\varepsilon = 10^{-7}$, $\theta = \pi/8$, $h = 0.01$.

As was expected, the numerical results show two interior layers along the characteristic lines emanating from the points of discontinuity of u_0 $(0, 0.25)$ and $(0, 0.5)$ at Γ_+ and a downstream boundary layer at the outflow side $x = 1$. It is seen, that no unphysical oscillations occur and the method is able to model the behavior of the exact solution accurately with no need to use any additional points in the layer domain.

5. Analysis of the numerical procedures

In this section we survey various techniques relevant to the present study, to prove stability and derive discretization error estimates. Since the rigorous error estimation is still a challenging problem requiring elaborate procedures, it is a subject of a separate publication. Here we restrict ourselves to heuristic explanation of the uniform convergence and stability of the method. We comment also shortly on the use of a hybrid method, i.e. a combination of the standard Galerkin and Petrov-Galerkin methods. As we shall see, it is the Petrov-Galerkin part, with proper test functions, which provides the stabilization of the methods.

5.1. Stability bounds. We recall first stability bounds for approximations of the problem (1.1) – (1.2). The first is associated with its variational formulation

$$(5.1) \quad a(u, v) = \int_{\Omega} f v d\Omega, \quad \text{for all } v \in H_0^1(\Omega)$$

where

$$a(u, v) = \int_{\Omega} (\varepsilon \nabla u \cdot \nabla v + \mathbf{b} \cdot \nabla u v + c u v) d\Omega,$$

and the norm

$$\|u\|_{1,\varepsilon} := [\varepsilon |u|_1^2 + \|u\|^2]^{\frac{1}{2}}.$$

For these, coercivity

$$\rho \|u\|_{1,\varepsilon}^2 \leq a(u, u) \quad \text{for all } u \in H_0^1(\Omega)$$

can be readily proven to hold with $\rho = \min\{1, c_0\}$ (see e.g. [3]) if

$$(5.2) \quad \min_{\Omega} (c - \frac{1}{2} \nabla \cdot \mathbf{b}) \geq c_0 > 0.$$

We shall assume that (5.2) holds and in addition, $c \geq 0$ in Ω . As shown in [3], even if the given velocity field \mathbf{b} does not satisfy (5.2), it can hold for a properly transformed differential equation. Together with the boundedness estimate

$$a(u, u) \leq \|f\| \|u\|,$$

it shows that there exists a unique solution, which satisfies $\|u\|_{1,\varepsilon} \leq \frac{1}{\rho} \|f\|$.

The other useful stability estimate follows from a local Green's function ψ_i , defined on the support ω_i of the corresponding local basis function φ_i , associated with the node \mathbf{x}_i :

$$(5.3) \quad \begin{aligned} \hat{\mathcal{L}}\psi_i &= \delta(\mathbf{x} - \mathbf{x}_i), \quad \mathbf{x} \in \omega_i \\ \psi_i|_{\partial\omega_i} &= 0 \end{aligned}$$

Assume that ψ_i is obtained explicitly from (5.3) in terms of normal derivatives $\varepsilon \frac{\partial \psi_i}{\partial n}|_{\partial\omega_i}$ in accordance with the scheme described in subsection 2.2. Then

$$\begin{aligned} \int_{\omega_i} f \psi_i d\Omega &= \int_{\omega_i} \mathcal{L}u \psi_i d\Omega = \\ &= \int_{\omega_i} (\varepsilon \nabla u \cdot \nabla \psi_i - \nabla \cdot (\mathbf{b} \psi_i) u + c u \psi_i) d\Omega + \oint_{\partial\omega_i} (\varepsilon \frac{\partial u}{\partial n} + \mathbf{b} \cdot \mathbf{n} u) \psi_i = \hat{a}(u, \psi_i), \end{aligned}$$

where

$$\hat{a}(u, v) = \int_{\omega_i} (\varepsilon \nabla u \cdot \nabla v - \nabla \cdot (\mathbf{b} v) u + c u v) d\Omega$$

Hence

$$\int_{\omega_i} f \psi_i d\Omega = \int_{\omega_i} (-\varepsilon \Delta \psi_i - \nabla \cdot (\mathbf{b} \psi_i) + c \psi_i) u d\Omega + \oint_{\partial\omega_i} \varepsilon \frac{\partial \psi_i}{\partial n} u,$$

or by (5.3),

$$(5.4) \quad u(\mathbf{x}_i) + \oint_{\partial\omega_i} \varepsilon \frac{\partial \psi_i}{\partial n} u = \int_{\omega_i} f \psi_i d\Omega, \quad i = 1, \dots, N.$$

Let now u be approximated by bilinear finite element functions and let u_h be the corresponding approximation also satisfying (5.4). For simplicity, we assume

that the integrals in (5.4) with u replaced by u_h can be computed exactly. It can be written in a matrix form

$$(5.5) \quad G_h \mathbf{U}_h = \mathbf{F}_h$$

where G_h is the corresponding finite element matrix and $\mathbf{U}_h, \mathbf{F}_h$ are the vectors corresponding to the nodal values of u_h and $\int_{\omega_i} f \psi_i$, respectively. When u_h is of form (1.3), (3.3) and ω_i are $2h \times 2h$ squares, we arrive naturally to the same system (3.1) with matrix $G_h = A = [a_{lk}]$ fixed by stencil (3.7).

If $\|G_h^{-1}\|_\infty$ is bounded by a constant C , independent of the number of node points and the aspect ratio of the elements, it follows from (5.5) that

$$(5.6) \quad \max_{\mathbf{x}_i \in \Omega_h} |u(\mathbf{x}_i)| = \|\mathbf{U}_h\|_\infty \leq C \|\mathbf{F}_h\|_\infty.$$

All numerical tests show that with $c > 0$ the matrix G_h is an M -matrix, so that elements of G_h^{-1} are bounded and non-negative. Analytically it can be proved for a potential vector field \mathbf{b} .

Theorem 5.1. *If coefficients of equation (1.1),(1.2) satisfy the following conditions in Ω :*

- 1) $c > 0$
- 2) \mathbf{b} is a potential vector field, that is, there exists a positive sufficiently smooth scalar function φ such that $\mathbf{b} = \nabla \varphi$ and $\varphi|_{\partial\Omega} \geq 0$
- 3) $|\mathbf{b}|^2 \geq b_0 > 0$
- 4) $\nabla \cdot \mathbf{b} \leq 0$.

Then G_h is a diagonally dominant M -matrix and $\|G_h^{-1}\| \leq \frac{\|\varphi\|_\infty}{b_0}$.

Proof. Since $\partial\psi_i/\partial n \leq 0$ on $\partial\omega_i$, the off-diagonal entries of G_h are non-positive. Diagonally dominant property follows from the fact that φ can be used as a barrier function. Note that $-\nabla \cdot \mathbf{b} = -\Delta\varphi$, therefore $\varphi \geq 0$. Then

$$(5.7) \quad \mathcal{L}\varphi = -\varepsilon\Delta\varphi + \mathbf{b} \cdot \nabla\varphi + c\varphi \geq |\mathbf{b}|^2 \geq b_0 \text{ in } \Omega.$$

As φ is a smooth function, it can be arbitrarily close approximated for sufficiently small values of h by finite element approximations φ_h , where

$$a(\varphi_h, v_h) = a(\varphi, v_h) \text{ for all } v_h \in V_h.$$

This discretization satisfies then (approximately) the same bound as in (5.5) and, in this case,

$$\|G_h^{-1}\| \leq \frac{\|\varphi_h\|_\infty}{b_0} \leq \frac{\|\varphi\|_\infty}{b_0},$$

where, due to the maximum principle, φ is bounded. □

5.2. Uniform convergence and a hybrid approach: preliminary arguments. To provide a proper background for the error estimation, we recall first the standard Galerkin method, which takes the form

$$a(u, v_h) = \int_{\Omega} f v_h d\Omega$$

or

$$a(u - u_h, v_h) = 0, \text{ for all } v_h \in V_h \subset H_0^1(\Omega),$$

where V_h is a finite element space. To estimate the discretization error $e_h = u - u_h$, we split it as $e_h = \eta - \theta_h$, where $\eta = u - u_{I_h}$, u_{I_h} is the interpolant to u on V_h and $\theta_h = u_h - u_{I_h}$. Then $a(\theta_h, \theta_h) = a(\eta, \theta_h)$ or, using coercivity,

$$\rho \|\theta_h\|_{1,\varepsilon}^2 \leq C[\varepsilon|\eta|_1^2 + \min\{\varepsilon^{-1/2}|\eta|, |\eta|_1\}^2 + \|\eta\|^2].$$

This shows that

$$\|\theta_h\|_{1,\varepsilon} < C \min\{\varepsilon^{-1/2}\|\eta\|_{1,\varepsilon^2}, \|\eta\|_1\}$$

and, by the triangle inequality,

$$\|e_h\|_{1,\varepsilon} \leq C \min\{\varepsilon^{-1/2}\|\eta\|_{1,\varepsilon^2}, \|\eta\|_1\}.$$

If $u \in H^{1+\nu}(\Omega)$, $0 < \nu \leq 1$ and if V_h is spanned by piecewise linear basis functions, we find then

$$\|u - u_h\|_{1,\varepsilon} \leq C \min\{\varepsilon^{1/2} + \varepsilon^{-1/2}h, h^\nu, h^\nu\} \|u\|_{1+\nu}.$$

In practice, however, due to boundary layers, the derivatives of the solution grow typically as $O(\varepsilon^{-1/2-\nu})$ as $\varepsilon \rightarrow 0$ and, unless $h \leq O(\varepsilon)$, this ε -dependence causes unphysical wiggles in the numerical solution, which spread into the whole domain. Therefore, one must use some cut-off weight function, which suppresses the influence of the layer part. Exponential weight functions were used in [3] and more general weight functions in [15] and [11]. It allows one to derive stable solutions and estimates in the layer free domain of $O(h)$, $h \rightarrow 0$ which holds uniformly in ε .

An alternative way to handle these oscillations is to use a Petrov-Galerkin method of the following form. Seek $u_h \in V_h$ such that

$$(5.8) \quad \hat{a}(u_h, v'_h) = \hat{a}(u, v'_h), \text{ for all } v'_h \in V'_h \subset H_0^1(\Omega),$$

where V_h is spanned by standard basis functions but V'_h in general by other basis functions. In particular, we are here interested in the case where V'_h contains local Green's functions.

As we have seen, due to the upwind shape of the local Green's functions, they work as cut-off functions. In particular, it suffices to use them in the layer domain, i.e. the Petrov-Galerkin method is used only there while the standard Galerkin method is used in Ω_{int} , the combination of them constituting a hybrid approach, which stabilizes the method.

An alternative heuristic explanation of this effect can be given using the classical Aubin-Nitsche duality argument. Given the solution u_h of the (hybrid) Petrov-Galerkin method in (5.7), we let φ be the solution of the adjoint equation,

$$\hat{\mathcal{L}}\varphi = u - u_h \text{ in } \Omega, \quad \frac{\partial \varphi}{\partial n} = 0 \text{ on } \partial\Omega$$

(assuming here for simplicity Dirichlet boundary conditions in (5.1)). Then

$$\int_{\Omega} (u - u_h)^2 d\Omega = \int_{\Omega} \hat{\mathcal{L}}\varphi (u - u_h) d\Omega$$

and a calculation shows that

$$\|u - u_h\|^2 = \int_{\Omega} [\varepsilon \nabla(u - u_h) \cdot \nabla(\varphi - v'_h) - \nabla \cdot \mathbf{b}(\varphi - v'_h)(u - u_h) + c(u - u_h)(\varphi - v'_h)] d\Omega.$$

We split the integral in two parts, $\int_{\Omega} = \int_{\Omega_0} + \int_{\Omega_1}$, where Ω_1 contains the boundary layer and $\Omega_0 = \Omega_{int}$. The direction of the flow for the adjoint equation is opposite to that of the given equation. Therefore, the function φ may have a layer at the inflow boundary but not at the outflow for the primal problem. This means that, locally, the factors $u - u_h$ and $\nabla \cdot (\mathbf{b}(\varphi - v'_h))$ and $\nabla(u - u_h)$ and $\nabla(\varphi - v'_h)$ can be expected to balance each other in Ω_0 and Ω_1 , respectively, so when one is big the other is correspondingly small. If V'_h contains fundamental solutions at an outflow layer, the corresponding local error $\varphi - v'_h$ is ε -independent and may even be zero. Hence, in this way, the boundary layers do not influence the global error.

6. Conclusion

For a 2D convection-diffusion problem we have demonstrated high practical efficiency of the local Green's function method (LGF) for the numerical solution of singularly perturbed problems when a semi-analytic technique of LGFs construction is developed. We propose to use a Fourier transform technique, which yields the LGFs in terms of 1D contour integrals with respect to the global Green's function and unknown normal derivatives at the boundary of LGF's supports. Analytical approximation of the latter in terms of orthogonal polynomials is derived from the integral equations in line with the Galerkin scheme.

The grid-discretization with the LGFs leads to sparse algebraic systems with M-matrices permitting the use of classical iterative solution methods. It becomes clear that the smaller the singular parameter is, the faster the convergence of the iterative solution is. In other words, the worse a singularly perturbed problem is, the more effective is the LGFM application for the iterative solution. In doing so, when an asymptotic calculation of the arising integrals is done, then the cost of obtaining the matrix-stencil becomes practically negligible.

Another way to reduce the cost spent for the construction of the LGFs for each mesh node with a variable coefficients problem is to use a hybrid method, where the standard Galerkin scheme is used in the major part of the domain, while the Petrov-Galerkin LGFM discretization is confined to subdomains where boundary or interior layers occur. The LGFM suppresses the well-known unphysical oscillations, which are inherent in the Galerkin method when it runs against the layer. Such a hybrid scheme, suggested in [3] for 1D problems, has to work in a multidimensional case as well.

For 3D problems the general scheme of the method remains the same. The local Green's function and the matrix-stencil are expressed in terms of unknown normal derivative on the mesh element surface, which is obtained from the boundary integral equations.

References

- [1] M. Abramowitz and I. A. Stegun, eds, Handbook of Mathematical Functions. Applied Mathematics Series 55, National Bureau of Standards, Washington D.C., 1964.
- [2] S. N. Atluri, S. Shen, The meshless local Petrov-Galerkin (MLPG) method: a simple & less-costly alternative to the finite element and boundary element methods, CMES: Computer Modeling in Engineering & Sciences, V. 3, No. 1 (2002) 11-51.
- [3] O. Axelsson, Stability and error estimates of Galerkin finite element approximations for convection-diffusion equations, IMA J. Numer. Anal., 1 (1981) 329-345.

- [4] O. Axelsson, A survey of numerical methods for convection-diffusion equations, In Proceedings of XIV National Summer School on Numerical Solution Methods, Varna, 29.8-3.9, 1988.
- [5] O. Axelsson, E. V. Glushkov, N. V. Glushkova, The Local Green's Function Method for Singularly Perturbed Convection-Diffusion Problems, Doklady Mathematics, V. 67, No 1 (2003) 98-102.
- [6] E. V. Glushkov, N. V. Glushkova, D. V. Timofeev, Solution of the singularly perturbed convection-diffusion problems by the local Green's functions method, 2004, submitted to Zhurnal Vychislitel'noy Matematiki i Matematicheskoy Fiziki (in Russian).
- [7] P. W. Hemker, A numerical study of stiff two-point boundary problems, Ph.D. thesis, Mathematical Center, Amsterdam, 1977.
- [8] P. W. Hemker, G. I. Shishkin, and L. P. Shishkina, ε -uniform schemes with high-order time-accuracy for parabolic singular perturbation problems, IMA J. Numer. Anal., 20, No. 1 (2000) 99-121.
- [9] T. J. R. Hughes et al., The variational multiscale method – a paradigm for computational mechanics, Comput. Methods. Appl. Mech. and Engrg. 166 (1998) 3-24.
- [10] T. J. R. Hughes, G. Scovazzi, and L. P. Franca, Multiscale and Stabilized Methods / in Encyclopedia of Computational Mechanics. Edited by E. Stein, R. de Borst and T.J.R. Hughes, John Wiley & Sons, Ltd., 2004.
- [11] C. Johnson, U. Nävert, and J. Pitkäranta, Finite element methods for linear hyperbolic problems, Comp. Meth. Appl. Mech. Eng., 45 (1984) 285-312.
- [12] D. Loghin, A.J. Wathen, Preconditioning the Advection-Diffusion Equation: the Green's Function Approach, Numerical Analysis Group Research Report NA-97/15, 1997 (<http://web.comlab.ox.ac.uk/oucl/publications/natr/na-97-15.html>).
- [13] J. E. Marsden and M. J. Hoffman, Basic Complex Analysis, Second ed., W.H.Freeman, New York, 1987.
- [14] K. W. Morton, Numerical Solution of Convection-Diffusion Problems, Chapman and Hall, London, 1996.
- [15] U. Nävert, A finite element method for convection-diffusion problems, Ph.D. thesis, Chalmers University of Technology, Göteborg, Sweden, 1982.
- [16] H. Roos, M. Stynes and L. Tobiska, Numerical Methods for Singularly Perturbed Differential Equations, Springer, Heidelberg, 1996.
- [17] R. S. Varga, Matrix Iterative Analysis, Englewood Cliffs, N.J., Prentice Hall, 1962.
- [18] L. S. Xanthis, C. Schwab, The method of arbitrary lines, C.R. Acad. Sci. Paris 312. Ser. I (1991) 181-187.

Faculty of Natural Sciences, Mathematics and Informatics, University of Nijmegen, Toernooiveld 1, NL 6525 ED Nijmegen, The Netherlands

E-mail: axelsson@sci.kun.nl

Department of Applied Mathematics, Kuban State University, P.O.Box 4102, Krasnodar, 350080, Russia

E-mail: evg@math.kubsu.ru and nvg@math.kubsu.ru

URL: <http://public.kubsu.ru/evg>